Chance-Constrained AC Optimal Power Flow for Distribution Systems with Renewables

Emiliano Dall'Anese, *Member*, *IEEE*, Kyri Baker, *Member*, *IEEE*, and Tyler Summers, *Member*, *IEEE*

***Abstract*—This paper focuses on distribution systems featuring renewable energy sources (RESs) and energy storage systems, and presents an AC optimal power flow (OPF) approach to optimize system-level performance objectives while coping with uncertainty in both RES generation and loads. The proposed method hinges on a chance-constrained AC OPF formulation where probabilistic constraints are utilized to enforce voltage regulation with prescribed probability. A computationally more affordable convex reformulation is developed by resorting to suitable linear approximations of the AC power-flow equations as well as convex approximations of the chance constraints. The approximate chance constraints provide conservative bounds that hold for arbitrary distributions of the forecasting errors. An adaptive strategy is then obtained by embedding the proposed AC OPF task into a model predictive control framework. Finally, a distributed solver is developed to strategically distribute the solution of the optimization problems across utility and customers.**

***Index Terms*—Distribution systems, renewable integration, optimal power flow, voltage regulation, model predictive control.**

I. Introduction

Systematic means to operate power distribution networks will be key to ensuring a reliable and efficient integration of renewable energy sources (RESs) and a sustainable capacity growth with limited need for system upgrade and expansion. By leveraging the increased flexibility offered by power-electronics-interfaced RESs, local inverter control strategies [1], [2] as well as network-wide optimization approaches [3], [4] are currently under development to alleviate emerging power-quality and reliability concerns that are precipitated by RESs operating with business-as-usual practices. For example, under reverse power flow conditions, inverter control and optimization approaches can decrease the likelihood of voltages violating prescribed limits [5].

RESs can be controlled alongside energy storage units to minimize the curtailment of renewable-based generation during overvoltage conditions and provide ancillary services to the grid. From the battery-owner perspective, benefits include increased self-consumption capabilities and the possibility of shaping the net load profile in response to market and pricing signals [1], [6].

E. Dall'Anese and K. Baker are with the National Renewable Energy Laboratory, Golden, CO. T. Summers is with the Department of Mechanical Engineering at University of Texas at Dallas. E-mails: emiliano.dallanese@nrel.gov, kyri.baker@nrel.gov, ths150130@utdallas.edu.

The work of E. Dall'Anese and K. Baker was supported by the Laboratory Directed Research and Development Program at the National Renewable Energy Laboratory and by the Grid Modernization Laboratory Consortium through project 1.4.10.

This paper examines network-wide optimization approaches to compute power setpoints based on forecasts of available RES generation and non-controllable loads. The proposed optimization method is based on a multi-period AC optimal power flow (OPF) formulation where probabilistic constraints are utilized to enforce voltage regulation with a prescribed probability. The nonlinearity of AC power flow equations and probabilistic constraints render stochastic (multi-period) AC OPF tasks computationally intractable [7], [8]. However, to enable a computationally feasible solution approach, an approximate reformulation of the AC OPF task is obtained by utilizing suitable linear approximations of the AC power flow equations [9]–[13] and pertinent convex approximations of the chance constraints [8], [14]. The approximate chance constraints provide conservative bounds that hold for arbitrary distributions of the forecasting errors, and render the overall problem deterministic and convex. An adaptive optimization strategy is then obtained by embedding the multi-period OPF task into a model predictive control (MPC) framework. Finally, a distributed solver is developed by utilizing the alternating direction method of multipliers (ADMM) [15], to enable utility and customers to pursue specific performance objectives, while achieving global coordination to ensure that voltage limits are systematically satisfied.

Prior works in context include e.g., [6] where an online energy control method for energy storages in grid-connected microgrids is developed and robust optimization arguments are leveraged to cope with load uncertainty; however, this approach does not consider voltage regulation as well as AC power-flow equations. A two-stage stochastic programming approach is utilized in [16] to solve an economic dispatch (based on a DC model) problem for microgrids, whereas MPC strategies are utilized in [17], [18] to dispatch energy storage commands. However, the approaches in [17], [18] do not model forecasting errors and are grounded on a DC model. A robust multi-period DC OPF problem is formulated in [19], while chance-constrained problem setups are considered in [20]–[23]. The approach of [21] enables a deterministic reformulation of the chance constraints when forecast errors are Gaussian distributed, while [20], [22] leverage conservative convex approximation of the chance constraints. General control policies are considered in [24], and deterministic reformulations of the probabilistic constraints in DC OPF settings are derived for Gaussian-distributed forecast errors in [23]. Overall, [20]–[24] offer means to deal with chance constraints in a computationally tractable way, but their applicability is limited to DC models. AC power flow models are considered in [25] where, however, forecasting errors are neglected, and in

[26], where RES-inverter commands are computed based on conditional value-at-risk arguments but energy storage systems and receding horizon control are not considered.

Overall, the present paper provides contributions in the following directions: i) a chance-constrained AC OPF problem is formulated where the RES and energy storage setpoints are optimized, while ensuring that voltages are within given limits with arbitrarily high probability; ii) existing linearization methods for the AC power-flow equations and conservative convex approximation of the (possibly nonconvex and computationally intractable) chance constraints are leveraged to derive a new computationally more efficient solution method for the formulated chance-constrained AC OPF task; and, iii) a distributed algorithm is developed where utility and customers agree on the setpoints while pursuing their own optimization objectives.

The remainder of the paper is organized as follows. Section II describes the network, inverter, and energy storage models and provides an overview of linear approximations of the AC power flow equations. Section III presents the proposed chance-constrained OPF strategy, while Section IV briefly outlines a distributed implementation of the AC OPF problem. Test cases are provided in Section V. Finally, Section VI concludes the paper.

II. Preliminaries and System model

A. System model

Consider a distribution feeder[1] comprising $N+1$ nodes collected in the set $\mathcal{N} \cup \{0\}$, $\mathcal{N} := \{1, \ldots, N\}$, and lines represented by the set of edges $\mathcal{E} := \{(m,n)\} \subset \mathcal{N} \times \mathcal{N}$. Let $V_n^t \in \mathbb{C}$ and $I_n^t \in \mathbb{C}$ denote the phasors for the line-to-ground voltage and the current injected at node $n \in \mathcal{N}$ at time t, respectively, and define the N-dimensional complex vectors $\mathbf{v}^t := [V_1^t, \ldots, V_N^t]^\mathsf{T} \in \mathbb{C}^N$ and $\mathbf{i}^t := [I_1^t, \ldots, I_N^t]^\mathsf{T} \in \mathbb{C}^N$. On the other hand, node 0 denotes the secondary of the distribution transformer, and it is taken to be the slack bus. Using Ohm's and Kirchhoff's circuit laws, the following linear relationship can be established:

$$\begin{bmatrix} I_0^t \\ \mathbf{i}^t \end{bmatrix} = \underbrace{\begin{bmatrix} y_{00} & \bar{\mathbf{y}}^\mathsf{T} \\ \bar{\mathbf{y}} & \mathbf{Y} \end{bmatrix}}_{:=\mathbf{Y}_{\text{net}}} \begin{bmatrix} V_0^t \\ \mathbf{v}^t \end{bmatrix} \tag{1}$$

where the system admittance matrix $\mathbf{Y}_{\text{net}} \in \mathbb{C}^{(N+1)\times(N+1)}$ is formed based on the system topology and the π-equivalent circuit of the distribution lines (see e.g., [27, Chapter 6] for additional details on distribution line modeling), and is partitioned in sub-matrices with the following dimensions: $\mathbf{Y} \in \mathbb{C}^{N \times N}$, $\bar{\mathbf{y}} \in \mathbb{C}^{N \times 1}$, and $y_{00} \in \mathbb{C}$. Finally, $V_0^t = \rho_0 e^{\mathrm{j}\theta_0}$ is the slack-bus voltage with ρ_0 denoting the voltage magnitude at the secondary of the step-down transformer.[2]

Let $P_{\ell,n}^t$ and $Q_{\ell,n}^t$ denote the non-controllable active and reactive demands at node $n \in \mathcal{N}$ at time t, and define the vectors $\mathbf{p}_\ell^t := [P_{\ell,1}^t, \ldots, P_{\ell,N}^t]^\mathsf{T}$ and $\mathbf{q}_\ell^t := [Q_{\ell,1}^t, \ldots, Q_{\ell,N}^t]^\mathsf{T}$. If no load is present at node n, then $P_{\ell,n}^t = Q_{\ell,n}^t = 0$, $\forall t$.

RES model. For given ambient conditions, let $P_{\text{av},n}^t$ denote the maximum renewable-based generation at node $n \in \mathcal{N}_R \subseteq \mathcal{N}$ at time t – hereafter referred to as the available active power. Particularly, $P_{\text{av},n}^t$ coincide with the maximum power point at the AC side of the inverter. When RESs operate at unity power factor and inject the available power $P_{\text{av},n}^t$, a set of challenges related to power quality and reliability in distribution systems may emerge for sufficiently high levels of deployed RES capacity [5]. For example, overvoltages may be experienced during periods when RES generation exceeds the household demand [5]. Efforts to ensure reliable operation of existing distribution systems with increased behind-the-meter RES generation are focused on the possibility of inverters providing reactive power compensation and/or curtailing active power. To account for the ability of the RES inverters to adjust the output active power, let $\alpha_n^t \in [0,1]$ denote the fraction of available active power curtailed by RES-inverters n at time t, and let Q_n^t be the reactive power provided by the same RES. With S_n denoting the rated apparent power, the possible setpoints for RES n at time t satisfy the following operational constraint:

$$((1-\alpha_n^t)P_{\text{av},n}^t)^2 + (Q_n^t)^2 \leq S_n^2 \,. \tag{2}$$

For future developments, it is convenient to define the vectors $\boldsymbol{\alpha}^t := [\alpha_1^t, \ldots, \alpha_N^t]^\mathsf{T}$, $\mathbf{p}_{\text{av}}^t := [P_{\text{av},1}^t, \ldots, P_{\text{av},N}^t]^\mathsf{T}$, and $\mathbf{q}_c^t := [Q_1^t, \ldots, Q_N^t]^\mathsf{T}$, with the convention that $\alpha_n^t = 0$, $P_{\text{av},n}^t = 0$, and $Q_n^t = 0$ for $n \in \mathcal{N} \backslash \mathcal{N}_R$.

Energy storage model. Let B_n^t represent the state of charge (SoC) of an energy storage system located at node $n \in \mathcal{N}_B \subseteq \mathcal{N}$, with the corresponding dynamical equation given by:

$$B_n^{t+1} = B_n^t + P_{B,n}^t \Delta^t \tag{3}$$

where Δ^t is the duration of slot $(t, t+1]$ and $P_{B,n}^t$ represents the power delivered to or drawn from the storage device. In particular, $P_{B,n}^t$ commands either the charging ($P_{B,n}^t > 0$) or the discharging ($P_{B,n}^t < 0$) of the battery during the time interval $(t, t+1]$. For simplicity, (3) presupposes that the round trip efficiency of the batteries is 1; however, once the analytical tools for dealing with non-convexity of the AC power flow equations as well as chance constraints are explained, a modified model for the batteries accounting for the round trip efficiency will be outlined in Remark 1. The operational limits of the storage device are as follows:

$$B_n^{\min} \leq B_n^t \leq B_n^{\max} \tag{4a}$$
$$P_{B,n}^{\min} \leq P_{B,n}^t \leq P_{B,n}^{\max} \tag{4b}$$

[1] Upper-case (lower-case) boldface letters will be used for matrices (column vectors); $(\cdot)^\mathsf{T}$ for transposition; $(\cdot)^*$ complex-conjugate; and, $(\cdot)^\mathsf{H}$ complex-conjugate transposition; $\Re\{\cdot\}$ and $\Im\{\cdot\}$ denote the real and imaginary parts of a complex number, respectively; $\mathrm{j} := \sqrt{-1}$ the imaginary unit; $|\cdot|$ denotes the absolute value of a number or the cardinality of a set; and, $\circ$ denotes Hadamard product. For $x \in \mathbb{R}$, function $[x]_+$ is defined as $[x]_+ := \max\{0, x\}$. Further, $\mathbb{I}_A(x)$ denotes the indicator function over the set $A \subset \mathbb{R}$; that is $\mathbb{I}_A(x) = 1$ if $x \in A$ and $\mathbb{I}_A(x) = 0$ otherwise. For a given $N \times 1$ vector $\mathbf{x} \in \mathbb{R}^N$, $\|\mathbf{x}\|_2 := \sqrt{\mathbf{x}^\mathsf{H}\mathbf{x}}$; $\text{diag}(\mathbf{x})$ returns a $N \times N$ matrix with the elements of $\mathbf{x}$ in its diagonal; and, $\mathbf{x} \succeq \mathbf{y}$ implies that the inequality $x_i \geq y_i$ is enforced for all the vector entries $i = 1, \ldots, N$. Finally, $\mathbf{I}_N$ denotes the $N \times N$ identity matrix; and, $\mathbf{0}_N$, $\mathbf{1}_N$ the N-dimensional vectors with all zeroes and ones, respectively, and $\mathbf{0}_{N\times M}$, $\mathbf{1}_{N\times M}$ are $N \times M$ matrices with all zeroes and ones.

[2] The admittance matrix is also time-varying due to possible system reconfigurations. However, for simplicity of exposition, we dropped the index t from admittances.

TABLE I
NOMENCLATURE

$\mathcal{N}$	Set of nodes $\{1,\ldots,N\}$
$\mathcal{N}_R$	Set of nodes with RESs
$\mathcal{N}_B$	Set of nodes with energy storage systems
V_n^t	Phasors for the voltage at node n at time t
ρ_n^t	Voltage magnitude at node n at time t
I_n^t	Current injected at node n at time t
$\mathbf{Y}_{\text{net}}$	System admittance matrix
$\bar{V}_n$	Linearization point for node n
$P_{\ell,n}^t + \mathrm{j}Q_{\ell,n}^t$	Demand at node $n \in \mathcal{N}$ at time t
$P_{\text{av},n}^t$	Available renewable generation at node n at time t
α_n^t	Fraction of active power curtailed by RES n at time t
Q_n^t	Reactive power provided by RES n at time t
S_n^t	Rated apparent power of RES n at time t
B_n^t	SoC of energy storage n at time t
$P_{B,n}^t$	Rate of (dis)charge for energy storage n at time t
$V^{\min}$	Lower limit for voltage magnitudes
$V^{\max}$	Upper limit for voltage magnitudes
$\mathcal{T}_t$	Interval $\{t, t+1, \ldots, t+T\}$
$\mathcal{T}_t'$	Interval $\{t, t+1, \ldots, t+T-1\}$
$\bar{\mathbf{p}}_{\text{av}}^\tau$	Forecasted values for $[P_{\text{av},1}^t, \ldots P_{\text{av},N}^t]^\mathsf{T}$
$\boldsymbol{\delta}_{\text{av}}^\tau$	Forecasting error for $[P_{\text{av},1}^t, \ldots P_{\text{av},N}^t]^\mathsf{T}$
$\bar{\mathbf{p}}_{\ell}^\tau$	Forecasted values for $[P_{\ell,1}^t, \ldots P_{\ell,N}^t]^\mathsf{T}$
$\bar{\mathbf{q}}_{\ell}^\tau$	Forecasted values for $[Q_{\ell,1}^t, \ldots Q_{\ell,N}^t]^\mathsf{T}$
$\boldsymbol{\delta}_{\ell}^\tau$	Forecasting error for loads
$g_{\rho,n}(\cdot)$	Entry n of the vector-valued function $\mathbf{g}_\rho(\cdot)$
ϵ	Probability of constraint violation for voltages
η	Probability of constraint violation for RES capacities
N_s	Number of samples

TABLE II
MAIN NOTATION

$$
\begin{aligned}
&\mathbf{v}^t := [V_1^t, \ldots, V_N^t]^\mathsf{T} \in \mathbb{C}^N\\
&\boldsymbol{\rho}^t := [|V_1^t|, \ldots, |V_N^t|]^\mathsf{T} \in \mathbb{R}^N\\
&\mathbf{i}^t := [I_1^t, \ldots, I_N^t]^\mathsf{T} \in \mathbb{C}^N\\
&\mathbf{p}_\ell^t := [P_{\ell,1}^t, \ldots, P_{\ell,N}^t]^\mathsf{T}\\
&\mathbf{q}_\ell^t := [Q_{\ell,1}^t, \ldots, Q_{\ell,N}^t]^\mathsf{T}\\
&\boldsymbol{\alpha}^t := [\alpha_1^t, \ldots, \alpha_N^t]^\mathsf{T}\\
&\mathbf{p}_{\text{av}}^t := [P_{\text{av},1}^t, \ldots, P_{\text{av},N}^t]^\mathsf{T}\\
&\mathbf{q}_c^t := [Q_1^t, \ldots, Q_N^t]^\mathsf{T}\\
&\mathbf{p}_B^t := [P_{B,1}^t, \ldots, P_{B,N}^t]^\mathsf{T}\\
&\mathbf{b}^t := [B_1^t, \ldots, B_N^t]^\mathsf{T}\\
&\boldsymbol{\delta}^t := (\mathbf{p}_{\text{av}}^t, \mathbf{p}_\ell^t, \mathbf{q}_\ell^t)\\
&\bar{\mathbf{v}} := [\bar{V}_1, \ldots, \bar{V}_N]^\mathsf{T}\\
&\mathbf{g}_\rho(\boldsymbol{\alpha}^t, \mathbf{q}_c^t, \mathbf{p}_B^t, \boldsymbol{\delta}^\tau) := \mathbf{R}((\mathbf{I} - \mathrm{diag}\{\boldsymbol{\alpha}\}^t)\mathbf{p}_{\text{av}}^t - \mathbf{p}_\ell^t + \mathbf{p}_B^t)\\
&\qquad\qquad + \mathbf{B}(\mathbf{q}_c^t - \mathbf{q}_\ell^t) + \mathbf{a}
\end{aligned}
$$

where $B_n^{\min}, B_n^{\max}$ are predetermined minimum and maximum SoC levels and $P_{B,n}^{\min}$ and $P_{B,n}^{\max}$ are minimum and maximum capacity limits. Additional constraints can be considered to accommodate user-defined requirements; for example, for an electric vehicle, the constraint $B_n^\tau = B_n^{\max}$ can be added to ensure that the battery is fully charged at a desired time τ. For future developments, define the vector $\mathbf{p}_B^t := [P_{B,1}^t, \ldots, P_{B,N}^t]^\mathsf{T}$ and $\mathbf{b}^t := [B_1^t, \ldots, B_N^t]^\mathsf{T}$, with the convention that $P_{B,n}^t = 0$ and $B_n^t = 0$ for the nodes $n \in \mathcal{N} \backslash \mathcal{N}_B$ where no energy storage systems are present.

Forecasting error model. The optimization problem that will be formulated in Section III considers a planning horizon $\mathcal{T}_t := \{t, t+1, \ldots, t+T\}$ of $T+1$ discrete time steps. To capture uncertainty in the ambient conditions as well as forecasting errors, $\mathbf{p}_{\text{av}}^\tau$, $\mathbf{p}_\ell^\tau$, and $\mathbf{q}_\ell^\tau$ are modeled as random variables [20], [22], [24]. Particularly, the available RES powers at time τ are modeled as $\mathbf{p}_{\text{av}}^\tau = \bar{\mathbf{p}}_{\text{av}}^\tau + \boldsymbol{\delta}_{\text{av}}^\tau$, where $\bar{\mathbf{p}}_{\text{av}}^\tau \in \mathbb{R}^N$ collects the forecasted values and $\boldsymbol{\delta}_{\text{av}}^\tau \in \mathcal{R}_{\text{av}}^\tau \subseteq \mathbb{R}^N$ is a random vector whose distribution captures spatial dependencies among forecasting errors. Similarly, the active and reactive loads at time $\tau \in \mathcal{T}_t$ are expressed as $\mathbf{p}_\ell^\tau = \bar{\mathbf{p}}_\ell^\tau + \mathbf{G}_p^\tau \boldsymbol{\delta}_\ell^\tau$ and $\mathbf{q}_\ell^\tau = \bar{\mathbf{q}}_\ell^\tau + \mathbf{G}_q^\tau \boldsymbol{\delta}_\ell^\tau$, respectively, where $\bar{\mathbf{p}}_\ell^\tau$ and $\bar{\mathbf{q}}_\ell^\tau$ are the forecasted loads; $\mathbf{G}_p^\tau, \mathbf{G}_q^\tau \in \mathbb{R}^{N \times J_\ell N}$ are model-dependent matrices; and, $\boldsymbol{\delta}_\ell^\tau \in \mathcal{R}_\ell^\tau \subseteq \mathbb{R}^{J_\ell N}$ is a random vector whose distribution captures spatial dependencies as well as correlations among active and reactive loads. We assume that the distribution system operator has a certain amount of information about the probability distributions of the forecasting errors $\boldsymbol{\delta}_{\text{av}}^\tau$ and $\boldsymbol{\delta}_\ell^\tau$ [20]–[22], [26]. This information can come in the form of either knowledge of the probability density functions, or a model of $\boldsymbol{\delta}_{\text{av}}^\tau$ and $\boldsymbol{\delta}_\ell^\tau$ from which one can draw samples. It is worth pointing out that the model set forth for the random parameters is flexible enough to handle any joint probability distributions; that is, possible correlations among (or independence of) random variables can be accounted for.

B. Leveraging approximate power-flow models

Using (1), the net complex-power injections can be compactly written as

$$\mathbf{s}^t = \mathrm{diag}\left(\mathbf{v}^t\right)\left(\mathbf{Y}^*(\mathbf{v}^t)^* + \bar{\mathbf{y}}^*(V_0^t)^*\right). \tag{5}$$

where $\mathbf{s}^t := [\mathbf{s}_1^t, \ldots, \mathbf{s}_N^t]^\mathsf{T}$ and $S_n^t = (1-\alpha_n^t)P_{\text{av},n}^t - P_{\ell,n}^t - P_{B,n}^t + \mathrm{j}(Q_n^t - Q_{\ell,n}^t)$. This equation typically appears in the form of a constraint in standard formulations of the OPF task, and renders the underlying optimization problem nonconvex [28]. Another source of nonconvexity in various OPF renditions is represented by the voltage-related constraint $V_{\min} \leq |V_n^t|$, where $V_{\min}$ represents a pre-determined lower limit for the voltage magnitude (e.g., ANSI C.84.1 limits). Non-convexity implies that off-the-shelf solvers for nonlinear programs may not achieve global optimality; from a computational standpoint, their complexity may become prohibitive with the increasing of the problem size [7]. Semidefinite relaxation techniques have been employed to bypass the nonconvexity of voltage-regulation and power-balance constraints, and yet achieve globally optimal solutions of the nonconvex OPF under a variety of conditions (see e.g., [28]). Several other convex relaxation techniques have also been investigated (see e.g., [29]–[31] and pertinent references therein). In this paper, to derive a reformulation of the multi-period OPF that is computationally more affordable, linear surrogates of (5) and voltage-regulation constraints will be sought next. Approximate power-flow relations will also facilitate the application of convex approximation techniques for chance constraints to the problem that will be formulated in Section III.

To this end, collect the voltage magnitudes $\{|V_n^t|\}_{n\in\mathcal{N}}$ in $\boldsymbol{\rho}^t := [|V_1^t|, \ldots, |V_N^t|]^\mathsf{T} \in \mathbb{R}^N$. The objective is to obtain approximate power-flow relations whereby voltages are *linearly* related to injected powers $\mathbf{s}^t$ as

$$\mathbf{v}^t \approx \mathbf{H}\mathbf{p}^t + \mathbf{J}\mathbf{q}^t + \mathbf{c} \quad (6)$$

$$\boldsymbol{\rho}^t \approx \mathbf{R}\mathbf{p}^t + \mathbf{B}\mathbf{q}^t + \mathbf{a}, \quad (7)$$

where $\mathbf{p}^t := \Re\{\mathbf{s}^t\}$ and $\mathbf{q}^t := \Im\{\mathbf{s}^t\}$. This way, voltage constraints $V^{\min} \leq |V_n^t| \leq V^{\max}$, $n \in \mathcal{N}$, can be approximated as $V^{\min}\mathbf{1}_N \preceq \mathbf{R}\mathbf{p}^t + \mathbf{B}\mathbf{q}^t + \mathbf{a} \preceq V^{\max}\mathbf{1}_N$, while (6)-(7) represents surrogates of (5).

The model parameters $\mathbf{R}, \mathbf{B}, \mathbf{H}, \mathbf{J}, \mathbf{a}$, and $\mathbf{c}$ in (6)–(7) can be obtained as explained in e.g., [9]–[13]. These works also provide bounds on the approximation errors. It is also worth noticing that the model (6)–(7) can be augmented with a random variable representing the approximation error (and the stochasticity can be handled in the chance-constraints explained in Section III). For illustration purposes, the approximation developed in [10], [12] is briefly described next.

Consider then linearizing the AC power-flow equation around a given voltage profile $\bar{\mathbf{v}} := [\bar{V}_1, \ldots, \bar{V}_N]^{\mathsf{T}}$. In the following, the voltages $\mathbf{v}$ satisfying the nonlinear power-balance equations (5) are expressed as $\mathbf{v} = \bar{\mathbf{v}} + \mathbf{e}$, where the entries of $\mathbf{e}$ capture deviations around the linearization points $\bar{\mathbf{v}}$. Collect in the vector $\bar{\boldsymbol{\rho}} \in \mathbb{R}_+^N$ the magnitudes of voltages $\bar{\mathbf{v}}$, and let $\bar{\boldsymbol{\gamma}} \in \mathbb{R}^N$ and $\bar{\boldsymbol{\mu}} \in \mathbb{R}^N$ collect elements $\{\cos(\bar{\theta}_n)\}$ and $\{\sin(\bar{\theta}_n)\}$, respectively, where $\bar{\theta}_i$ is the angle of the nominal voltage $\bar{V}_i$. Expanding on (5), and discarding second-order term $\mathrm{diag}\,(\mathbf{e})\,\mathbf{Y}^*\mathbf{e}^*$, it turns out that (5) can be approximated as $\boldsymbol{\Gamma}\mathbf{e} + \boldsymbol{\Phi}\mathbf{e}^* = \mathbf{s} + \boldsymbol{\upsilon}$, where $\boldsymbol{\Gamma} := \mathrm{diag}\,(\mathbf{Y}^*\bar{\mathbf{v}}^* + \bar{\mathbf{y}}^*V_0^*)$, $\boldsymbol{\Phi} := \mathrm{diag}\,(\bar{\mathbf{v}})\,\mathbf{Y}^*$, and $\boldsymbol{\upsilon} := -\mathrm{diag}\,(\bar{\mathbf{v}})\,(\mathbf{Y}^*\bar{\mathbf{v}}^* + \bar{\mathbf{y}}^*V_0^*)$. Next, consider then the following choice of the nominal voltage $\bar{\mathbf{v}}$:

$$\bar{\mathbf{v}} = -\mathbf{Y}^{-1}\bar{\mathbf{y}}V_0\,. \quad (8)$$

Using (8), it follows that $\boldsymbol{\Gamma} = \mathbf{0}_{N\times N}$ and $\boldsymbol{\upsilon} = \mathbf{0}_N$, and therefore one obtains the linearized power-flow expression

$$\mathrm{diag}\,(\bar{\mathbf{v}}^*)\,\mathbf{Y}\mathbf{e} = \mathbf{s}^*. \quad (9)$$

Notice that matrix $\mathbf{Y}$ is diagonally dominant and irreducible [10]. Particularly, it is diagonally dominant by construction since $|y_{ii}| \geq \sum_{n\neq i}|y_{in}|$ for all $n \in \mathcal{N}$; it is also irreducibly diagonally dominant if $|y_{0i}| > 0$ for any i. Then, a solution to (9) can be expressed as $\mathbf{e} = \mathbf{Y}^{-1}\mathrm{diag}^{-1}(\bar{\mathbf{v}}^*)\mathbf{s}^*$. Thus, expanding on this relation, the approximate voltage-power relationship (6) can be obtained by defining the matrices:

$$\bar{\mathbf{R}} = \mathbf{Z}_R\mathrm{diag}(\bar{\boldsymbol{\gamma}})(\mathrm{diag}(\bar{\boldsymbol{\rho}}))^{-1} - \mathbf{Z}_I\mathrm{diag}(\bar{\boldsymbol{\mu}})(\mathrm{diag}(\bar{\boldsymbol{\rho}}))^{-1} \quad (10a)$$

$$\bar{\mathbf{B}} = \mathbf{Z}_I\mathrm{diag}(\bar{\boldsymbol{\gamma}})(\mathrm{diag}(\bar{\boldsymbol{\rho}}))^{-1} + \mathbf{Z}_R\mathrm{diag}(\bar{\boldsymbol{\mu}})(\mathrm{diag}(\bar{\boldsymbol{\rho}}))^{-1} \quad (10b)$$

where $\mathbf{Z}_R := \Re\{\mathbf{Y}^{-1}\}$ and $\mathbf{Z}_I := \Im\{\mathbf{Y}^{-1}\}$, and setting $\mathbf{H} = \bar{\mathbf{R}} + \mathrm{j}\bar{\mathbf{B}}$, $\mathbf{J} = \bar{\mathbf{B}} - \mathrm{j}\bar{\mathbf{R}}$, and $\mathbf{c} = \bar{\mathbf{v}}$. If the entries of $\bar{\mathbf{v}}$ dominate those in $\mathbf{e}$, then $\bar{\boldsymbol{\rho}} + \Re\{\mathbf{e}\}$ serves as a first-order approximation to the voltage magnitudes across the distribution network [10], and relationship (7) can be obtained by setting $\mathbf{R} = \bar{\mathbf{R}}$, $\mathbf{B} = \bar{\mathbf{B}}$, and $\mathbf{a} = \bar{\boldsymbol{\rho}}$. Equations (6)–(7) will be utilized next to develop a computationally affordable multi-period OPF strategy.

III. Computation of RES and battery setpoints

A multi-period OPF problem optimizing the operation of a distribution system over the interval $\mathcal{T}_t$ is formulated first, and subsequently utilized as a building block for an MPC strategy. At time instant t, the objective of the distribution system operator is to compute the setpoints $\{\boldsymbol{\alpha}^t, \mathbf{q}_c^t\}$ for the RES inverters as well as to adaptively schedule the SoC of the batteries via the variables $\mathbf{p}_B^t, \mathbf{b}^t$ so that well-defined performance objectives are maximized, while concurrently ensuring that voltage limits are satisfied. To this end, forecasts for $\boldsymbol{\delta}^\tau := (\mathbf{p}_{\text{av}}^\tau, \mathbf{p}_\ell^\tau, \mathbf{q}_\ell^\tau), \tau = t, \ldots, t+T$ are available. For brevity, define the following vector-valued function [cf. (6)–(7)]:

$$\begin{aligned}\mathbf{g}_\rho(\boldsymbol{\alpha}^t, \mathbf{q}_c^t, \mathbf{p}_B^t, \boldsymbol{\delta}^\tau) :=& \mathbf{R}((\mathbf{I} - \mathrm{diag}\{\boldsymbol{\alpha}\}^t)\mathbf{p}_{\text{av}}^t - \mathbf{p}_\ell^t - \mathbf{p}_B^t) \\ &+ \mathbf{B}(\mathbf{q}_c^t - \mathbf{q}_\ell^t) + \mathbf{a}\,.\end{aligned}$$

Consider then the following optimization problem:

$$\begin{aligned}
&(\text{P0}) \quad \min_{\{\boldsymbol{\alpha}^\tau, \mathbf{q}_c^\tau, \mathbf{p}_B^\tau, \mathbf{b}^\tau\}} \sum_{\tau=t}^{t+T} \mathbb{E}[C^\tau(\boldsymbol{\alpha}^\tau, \mathbf{q}_c^\tau, \mathbf{p}_B^\tau, \boldsymbol{\delta}^\tau)] && \text{(11a)}\\
&\text{subject to}\\
&\Pr\{g_{\rho,n}(\boldsymbol{\alpha}^\tau, \mathbf{q}_c^\tau, \mathbf{p}_B^\tau, \boldsymbol{\delta}^\tau) \leq V_{\max}\} \geq 1 - \epsilon\\
&\qquad\qquad \forall\, n \in \mathcal{N}, \tau \in \mathcal{T}_t && \text{(11b)}\\
&\Pr\{V_{\min} \leq g_{\rho,n}(\boldsymbol{\alpha}^\tau, \mathbf{q}_c^\tau, \mathbf{p}_B^\tau, \boldsymbol{\delta}^\tau)\} \geq 1 - \epsilon\\
&\qquad\qquad \forall\, n \in \mathcal{N}, \tau \in \mathcal{T}_t && \text{(11c)}\\
&\Pr\{((1-\alpha_i^\tau)P_{\text{av},i}^\tau)^2 + (Q_i^\tau)^2 \leq S_i^2\,\} \geq 1 - \eta\\
&\qquad\qquad \forall\, i \in \mathcal{N}_R, \tau \in \mathcal{T}_t && \text{(11d)}\\
&0 \leq \alpha_i^\tau \leq 1 \qquad \forall\, i \in \mathcal{N}_R, \tau \in \mathcal{T}_t && \text{(11e)}\\
&B_j^{\tau+1} = B_j^\tau + P_{B,j}^\tau\Delta^t \qquad \forall\, j \in \mathcal{N}_B, \tau \in \mathcal{T}_t' && \text{(11f)}\\
&P_{B,j}^{\min} \leq P_{B,j}^\tau \leq P_{B,j}^{\max} \qquad \forall\, j \in \mathcal{N}_B, \tau \in \mathcal{T}_t' && \text{(11g)}\\
&B_j^{\min} \leq B_j^{t+1} \leq B_j^{\max} \qquad \forall\, j \in \mathcal{N}_B, \tau \in \mathcal{T}_t' && \text{(11h)}
\end{aligned}$$

where $g_{\rho,n}(\cdot)$ denotes the n-th element of the vector-valued function $\mathbf{g}_\rho(\cdot)$ and $\mathcal{T}_t' := \{t, \ldots, t+T-1\}$. Constraints (11g)–(11h) optimize the RES and battery utilization over the whole horizon. Given the predicted values of both available powers $\{\bar{\mathbf{p}}_{\text{av}}^\tau\}_{\tau\in\mathcal{T}_t}$ and loads $\{\bar{\mathbf{p}}_\ell^\tau, \bar{\mathbf{q}}_\ell^\tau\}_{\tau\in\mathcal{T}_t}$, along with the associated forecasting errors, the chance constraints (11b)–(11d) ensure that RES and battery setpoints can be scheduled in a way that inverter capacity limits and voltage limits are satisfied with prescribed probabilities $1-\eta$ and $1-\epsilon$, respectively. Functions $\{C^\tau(\cdot)\}_{\tau\in\mathcal{T}_t}$ are convex and model e.g., expected (reward for) ancillary service provisioning, feed-in tariffs, cycling of batteries, and other economic performance indicators [3], [4], [10]. Of particular relevance is the minimization of the active power curtailed, which promotes utilization of RES-based generation, while concurrently respecting voltage limits. Notice that one can also show that the power losses can be expressed as a convex function of active and reactive power via (6) (see e.g., [10]).

Constraints (11b)–(11c) are, however, problematic. It may turn out that the feasible set of (11b)–(11d) is nonconvex. For example, (11b)–(11c) are convex and efficiently manageable only when $\boldsymbol{\delta}^\tau$ is the image, under affine transformation, of a random vector with rotationally invariant distribution – with the multivariate Gaussian distribution as a prime example (see e.g., [8]).

To account for a variety of possible distributions of the forecasting errors $\boldsymbol{\delta}^\tau$ and yet derive a computationally efficient solution method for the stochastic multi-period OPF, a convex approximation of the chance constraints is pursued next. Summarizing, this paper leverages: 1) linear approximation of the AC power-flow equations to bypass the non-convexity of the balance equations and voltage constraints in AC OPF problems; and, 2) the techniques in [8] to derive conservative convex approximations of infinite-dimensional (and possibly non-convex) chance constraints.

A. Leveraging convex approximation of chance constraints

Consider the generic scalar chance constraint $\Pr\{g(\mathbf{x}, \boldsymbol{\delta}) > 0\} \leq \epsilon$, where function $g(\mathbf{x}, \boldsymbol{\delta})$ is convex in the optimization variables $\mathbf{x}$ for given values of the random vector $\boldsymbol{\delta}$. Key to developing a conservative convex approximation for this chance constraint, is to consider a function $\psi : \mathbb{R} \to \mathbb{R}$ that is nonnegative valued, nondecreasing, and convex. Further, assume that $\psi(\cdot)$ – henceforth referred to as the (one-dimensional) generating function – satisfies the conditions $\psi(x) > \psi(0)\ \forall x > 0$ and $\psi(0) = 1$. Given a positive scalar $z > 0$ and a random variable δ, it holds that: $\mathbb{E}_\delta\{\phi(z^{-1}\delta)\} \geq \mathbb{E}_\delta\{\mathbb{I}_{[0,+\infty)}(z^{-1}\delta)\} = \Pr\{z^{-1}\delta \geq 0\} = \Pr\{\delta \geq 0\}$, where $\mathbb{E}_\delta$ denotes expectation with respect to δ. Thus, by taking $\delta = g(\mathbf{x}, \boldsymbol{\delta})$ one has that the following bound holds for all $z > 0$ and $\mathbf{x}$ [8]:

$$\Pr\{g(\mathbf{x}, \boldsymbol{\delta}) > 0\} \leq \mathbb{E}_{\boldsymbol{\delta}}\left\{\psi\left(z^{-1}g(\mathbf{x}, \boldsymbol{\delta})\right)\right\} . \tag{12}$$

It follows that the constraint

$$\inf_{z>0}\left\{z\mathbb{E}_{\boldsymbol{\delta}}\left\{\psi(z^{-1}g(\mathbf{x}, \boldsymbol{\delta}))\right\} - z\epsilon\right\} \leq 0 \tag{13}$$

represents a sufficient condition for $\Pr\{g(\mathbf{x}, \boldsymbol{\delta}) > 0\} \leq \epsilon$ and hence is also a conservative convex approximation of the chance constraint $\Pr\{g(\mathbf{x}, \boldsymbol{\delta}) \leq 0\} \geq 1 - \epsilon$. Regarding the convexity of (13), notice that since $\psi(\cdot)$ is nondecreasing and convex and $g(\cdot, \boldsymbol{\delta})$ is convex, it follows that the mapping $(\mathbf{x}, z) \to z\psi(z^{-1}g(\mathbf{x}, \boldsymbol{\delta}))$ is convex. If g is biaffine in $\mathbf{x}$ and $\boldsymbol{\delta}$ and ψ is quadratic, then the constraint (13) is also convex.

Next, consider the piecewise linear function $\psi(x) = [1 + x]_+$. In this case, the approximate constraint (13) takes the following form:

$$\inf_{z\in\mathbb{R}} \mathbb{E}_{\boldsymbol{\delta}}\left\{[g(\mathbf{x}, \boldsymbol{\delta}) + z]_+\right\} - z\epsilon \leq 0 \tag{14}$$

where the infimum is taken over $z \in \mathbb{R}$ (instead of the non-negative orthant) without compromising the validity of the bound. It turns out that (14) is closely related to the concept of conditional value at risk (CVaR), which is a well-known coherent risk measure in risk management and optimization under uncertainty [8], [22], [26].

Thus, replacing the generic convex function $g(\mathbf{x}, \boldsymbol{\delta})$ with $g_{\rho,n}(\boldsymbol{\alpha}^\tau, \mathbf{q}_c^\tau, \mathbf{p}_B^\tau, \boldsymbol{\delta}^\tau) - V_{\max}$ and $V_{\min} - g_{\rho,n}(\boldsymbol{\alpha}^\tau, \mathbf{q}_c^\tau, \mathbf{p}_B^\tau, \boldsymbol{\delta}^\tau)$, respectively, it follows that CVaR-type convex approximations of (11b)–(11c) amount to:

$$\mathbb{E}_{\boldsymbol{\delta}^\tau}\left\{[g_{\rho,n}(\boldsymbol{\alpha}^\tau, \mathbf{q}_c^\tau, \mathbf{p}_B^\tau, \boldsymbol{\delta}^\tau) - V_{\max} + z_n^\tau]_+\right\} \leq z_n^\tau\epsilon \tag{15}$$

$$\mathbb{E}_{\boldsymbol{\delta}^\tau}\left\{[V_{\min} - g_{\rho,n}(\boldsymbol{\alpha}^\tau, \mathbf{q}_c^\tau, \mathbf{p}_B^\tau, \boldsymbol{\delta}^\tau) + y_n^\tau]_+\right\} \leq y_n^\tau\epsilon \tag{16}$$

where $\{z_n^\tau \in \mathbb{R}_+\}_{n,\tau}$ and $\{y_n^\tau \in \mathbb{R}_+\}_{n,\tau}$ will be auxiliary optimization variables. Similarly, setting $g(\mathbf{x}, \boldsymbol{\delta})$ to $((1 - \alpha_n^\tau)P_{\text{av},n}^\tau)^2 + (Q_n^\tau)^2 - S_n^2$, (11d) can be approximated as

$$\mathbb{E}_{\boldsymbol{\delta}^\tau}\left\{\left[((1 - \alpha_n^\tau)P_{\text{av},n}^\tau)^2 + (Q_n^\tau)^2 - S_n^2 + x_n^\tau\right]_+\right\} \leq x_n^\tau\eta \tag{17}$$

where $\{x_n^\tau \in \mathbb{R}_+\}_{n,\tau}$ will be auxiliary optimization variables. An advantage of (15)–(17) is that empirical estimates of the expected values can be obtained via sample averaging. Accordingly, given N_s samples $\{\boldsymbol{\delta}^\tau[s]\}_{s=1}^{N_s}$, of the random vector $\boldsymbol{\delta}^\tau$, an approximation of (15)–(17) for arbitrary distributions can be accommodated in the OPF task as follows:

$$\text{(P1)} \min_{\substack{\{\boldsymbol{\alpha}^\tau, \mathbf{q}_c^\tau, \mathbf{p}_B^\tau, \mathbf{b}^\tau\} \\ \{w^\tau\}, \{x_n^\tau, z_n^\tau, y_n^\tau\}}} \sum_{\tau=t}^{t+T} w^\tau$$

$$\text{subject to (11e)} - \text{(11h), and}$$

$$\frac{1}{N_s}\sum_{s=1}^{N_s} C^\tau(\boldsymbol{\alpha}^\tau, \mathbf{q}_c^\tau, \mathbf{p}_B^\tau, \boldsymbol{\delta}^\tau[s]) \leq w^\tau \quad \forall \tau \in \mathcal{T}_t \tag{18a}$$

$$\frac{1}{N_s}\sum_{s=1}^{N_s}\left[((1 - \alpha_i^\tau)P_{\text{av},i}^\tau[s])^2 + (Q_i^\tau)^2 - S_i^2 + x_i^\tau\right]_+ \leq x_i^\tau\eta \qquad \forall\, i \in \mathcal{N}_R, \tau \in \mathcal{T}_t \tag{18b}$$

$$\frac{1}{N_s}\sum_{s=1}^{N_s}[g_{\rho,n}(\boldsymbol{\alpha}^\tau, \mathbf{q}_c^\tau, \mathbf{p}_B^\tau, \boldsymbol{\delta}^\tau[s]) - V_{\max} + z_n^\tau]_+ \leq z_n^\tau\epsilon \qquad \forall\, n \in \mathcal{N}, \tau \in \mathcal{T}_t \tag{18c}$$

$$\frac{1}{N_s}\sum_{s=1}^{N_s}[V_{\min} - g_{\rho,n}(\boldsymbol{\alpha}^\tau, \mathbf{q}_c^\tau, \mathbf{p}_B^\tau, \boldsymbol{\delta}^\tau[s]) + y_n^\tau]_+ \leq y_n^\tau\epsilon \qquad \forall\, n \in \mathcal{N}, \tau \in \mathcal{T}_t\,. \tag{18d}$$

For a sufficiently high number of samples N_s, almost sure convergence of the sample averages on the left hand side of (18b)-(18d) to $\mathbb{E}_{\boldsymbol{\delta}^\tau}\{[((1 - \alpha_i^\tau)P_{\text{av},i}^\tau)^2 + (Q_i^\tau)^2 - S_i^2 + x_i^\tau]_+\}$, $\mathbb{E}_{\boldsymbol{\delta}^\tau}\{[g_{\rho,n}(\boldsymbol{\alpha}^\tau, \mathbf{q}_c^\tau, \mathbf{p}_B^\tau, \boldsymbol{\delta}^\tau) - V_{\max} + z_n^\tau]_+\}$ and $\mathbb{E}_{\boldsymbol{\delta}^\tau}\{[V_{\max} - g_{\rho,n}(\boldsymbol{\alpha}^\tau, \mathbf{q}_c^\tau, \mathbf{p}_B^\tau, \boldsymbol{\delta}^\tau) + y_n^\tau]_+\}$, respectively, can guaranteed by using large deviations theory [32]–[34]. Furthermore, sample average approximation methods with modest numbers of samples have been shown to be effective in many practical problems [34], [35].

Regarding the approximate problem (18), the following points should be stressed: *i)* (P1) is a convex program; *ii)* the number of optimization variables does not increase with the increasing of the number of samples N_s; and, *iii)* any distribution of the random vectors $\mathbf{p}_{\text{av}}^\tau$, $\mathbf{p}_\ell^\tau$, and $\mathbf{q}_\ell^\tau$ can be accommodated in (P1). In particular, arbitrary distributions can be accommodated so long as one has a mechanism from which to draw samples of $\boldsymbol{\delta}_{\text{av}}^\tau$ and $\boldsymbol{\delta}_\ell^\tau$.

B. Model predictive control implementation

When determining the control decisions for devices with intertemporal constraints (e.g., energy storage units), it is advantageous to not only take into account the current time step, but also potential future system states. MPC is an adaptive control technique that enacts optimal control decisions in the current time step while taking into account the system behavior over a chosen time horizon [16]–[18]. In the present context, problem (P1) constitutes a building block for a MPC-based strategy that adapts current and future setpoints based on forecasts of available RES powers and loads. Particularly, the MPC strategy involves the following steps:

[A1] At time instant t, acquire the forecasting of available RES power and loads over $\mathcal{T}_t$.
[A2] Solve (P1) over the horizon $\mathcal{T}_t$.
[A3] Send setpoints $\{\alpha_i^t, Q_i^t\}_{i\in\mathcal{N}_R}$ to the RES inverters and send commands $\{P_{B,i}^t\}_{i\in\mathcal{N}_B}$ to batteries.
[A4] $\mathcal{T}_t \rightarrow \mathcal{T}_{t+1}$, and go to step [A1].

Once the optimal setpoints are calculated for the entire time horizon $\mathcal{T}_t$, the control decisions for the current step are applied to RES and battery units. Then, the forecasts are updated, and the time window is shifted by a time slot.

In Section IV, a distributed algorithm is proposed to decompose the optimization task [A2] across utility and customers. But first, a few remarks are in order.

Remark 1 (Battery efficiency). For simplicity, no charging/discharging losses were considered in the dynamical equation of the energy storage (3) [25]. However, charging and discharging efficiencies can be readily incorporated in (3) and (11f), at the cost of increasing the complexity of problems (P0) – (P1). To this end, let $\eta_c \in (0,1]$ and $\eta_d \in (0,1]$ denote the charging and discharging efficiencies, respectively; further, let $P_{B_c,n}^t \geq 0$ denote the power supplied to the battery n, and $P_{B_d,n}^t \geq 0$ the power withdrawn from the battery. With these definitions, (3) can be modified as [36]:

$$B_n^{t+1} = B_n^t + \eta_c P_{B_c,n}^t \Delta^t - \frac{1}{\eta_d} P_{B_d,n}^t \Delta^t. \tag{19}$$

Clearly, at any time t, $P_{B_c,n}^t$ and $P_{B_d,n}^t$ cannot be concurrently greater than zero (i.e., the battery cannot be simultaneously charged and discharged). To this end, it is necessary to add in problems (P0) – (P1) additional constraints; particularly, one can either i) add binary variables that indicate whether the battery is charging or discharging [19], or, ii) add the constraint $P_{B_c,n}^t P_{B_d,n}^t = 0$. Either way, with these additional constraints problem (P1) would become nonconvex. However, when the constraint $P_{B_c,n}^t P_{B_d,n}^t = 0$ is considered, successive convex approximation techniques can be utilized to identify a (possibly locally optimal) solution of (P1). Alternatively, mixed-integer solvers could be used with binary variables, though this poses practical difficulties in medium to large problems and in distributed settings. On the other hand, to preserve convexity of (P1), prior works in context considered replacing (11f) with (19) and disregarding the nonconvex constraint $P_{B_c,n}^t P_{B_d,n}^t = 0$ [36].

Remark 2 (Policy for RES inverters). Similar to e.g., [22], [24], model (11e) (and, hence, (18b)) dictates an adaptive policy for the setpoints commanded to the RES inverters to accommodate the uncertainty in $\boldsymbol{\delta}_{\text{av}}^t$. In fact, once α_n^t is computed, inverter n will curtail $\alpha_n^t P_{\text{av},n}^t$ during the time interval $(t, t+1]$. Regarding Q_n^t, if the setpoint $((1-\alpha_n^t)P_{\text{av},n}^t, Q_n)$ is outside the inverter operating region [cf. (11e)], the value of Q_n^t can be reduced to adhere to the capacity limits of the inverter.

Remark 3 (Recursive feasibility). The basic implementation described above does not necessarily provide recursive feasibility, where feasibility of the optimization problem at each time step is guaranteed if the problem is initially feasible. Recursive feasibility in stochastic model predictive control is a major challenge and an active research topic. More elaborate techniques from the recent literature may be applied to provide recursive feasibility under certain conditions [37].

Remark 4 (Multi-phase systems). For notational and exposition simplicity, the paper considers a balanced distribution network. However, the proposed framework is readily applicable to multi-phase unbalanced systems with any topology. In fact, the linearized model in Section II-B can be extended to the multi-phase unbalanced setup, and the optimization problems can be modified to accommodate chance-constraints on each phase and node.

Remark 5 (Flow limits). Using the linear approximation developed in [10], [12], it is possible to derive an (approximate) linear relationship between voltage angles and net injected powers as:

$$\boldsymbol{\theta}^t \approx \mathbf{N}\mathbf{p}^t + \mathbf{M}\mathbf{q}^t + \mathbf{d} \tag{20}$$

where $\boldsymbol{\theta}^t \in \mathbb{R}^N$ collects the voltage angles on the nodes and $\mathbf{N}$, $\mathbf{M}$, and $\mathbf{d}$ can be built from (6). The approximation (20) can be utilized to impose line flow limits in the OPF problem without increasing the underlying computational complexity. Particularly, let θ^{max} be a maximum phase shift over a line; then, the following constraints can be included in (P0) to account for power flows on each line:

$$\Pr\{|\theta_i - \theta_j| \leq \theta^{max}\} \geq 1 - \epsilon \tag{21}$$

where $\epsilon > 0$ is a pre-defined parameter. Substituting (20) into (21) and utilizing (14), a deterministic convex approximation of (21) can be obtained. The resultant approximation can be included in problem (P1).

IV. Distributed implementation

A distributed solution of the convex problem (P1) is developed next in order to enable utility and customers to pursue specific performance objectives, while ensuring that voltage limits are systematically satisfied. For example, customer-based optimization includes minimizing the cost when feed-in tariffs are applied [1] and/or maximizing the revenue from ancillary service provisioning [3], [4]; customers retain controllability of their RES and battery systems, and optimize the utilization of these devices subject to the operational constraints (11f)–(11h) and (18b). On the other hand, objectives of the utility may include e.g., minimization of the power losses as well as adherence to voltage limits. For simplicity of notation, assume that RESs and batteries are co-located at nodes

$\mathcal{N}_C \subseteq \mathcal{N}$; the algorithm clearly handles the general case where some RESs and batteries are not co-located. Then, consider decoupling the cost function in (18) as $C^\tau(\boldsymbol{\alpha}^\tau, \mathbf{q}_c^\tau, \mathbf{p}_B^\tau, \boldsymbol{\delta}^\tau) = C_u^\tau(\boldsymbol{\alpha}^\tau, \mathbf{q}_c^\tau, \mathbf{p}_B^\tau, \boldsymbol{\delta}^\tau) + \sum_{n \in \mathcal{N}_C} C_{c,n}^\tau(\boldsymbol{\alpha}^\tau, \mathbf{q}_c^\tau, \mathbf{p}_B^\tau, \boldsymbol{\delta}^\tau)$, where $C_u^\tau(\cdot)$ captures utility-oriented performance target and $C_{c,n}^\tau(\cdot)$ models the optimization objectives of the nth customer. For notational simplicity, define the vector $\mathbf{u}_n^\tau := [\alpha_n^\tau, Q_n^\tau, P_{B,n}^\tau]^\mathsf{T}$ collecting the setpoints for the RES and the battery located at node n.

The distributed solution developed in this section leverages the ADMM techniques [15, Sec. 3.4]. Notice however that the presence of samples $\{\boldsymbol{\delta}^\tau[s]\}$ in the probabilistic constraints may require adding a set of auxiliary optimization variables per sample $s = 1, \ldots, N_s$ to enable a decomposition of the solution of (P1) across utility and customers. To bypass this hurdle, one way is to introduce the (sample-independent) auxiliary variables $\tilde{\mathbf{u}}_n^\tau$, which represent *copies* of the setpoints $\mathbf{u}_n^\tau$ at the utility, for all $n \in \mathcal{N}$ and $\tau \in \mathcal{T}$. Accordingly, (P1) can be re-stated in the following equivalent way:

$$\text{(P2)} \min_{\substack{\{\tilde{\mathbf{u}}^\tau, \mathbf{u}^\tau, \mathbf{b}^\tau\} \\ \{w_n^\tau\}, \{\tilde{w}^\tau\} \\ \{x_n^\tau, z_n^\tau, y_n^\tau\}}} \sum_{\tau=t}^{t+T} \left(\tilde{w}^\tau + \sum_{i \in \mathcal{N}_C} w_i^\tau \right)$$

$$\text{subject to}$$

$$\frac{1}{N_s} \sum_{s=1}^{N_s} C_u^\tau(\tilde{\mathbf{u}}^\tau, \boldsymbol{\delta}^\tau[s]) \leq \tilde{w}^\tau \tag{22a}$$

$$\frac{1}{N_s} \sum_{s=1}^{N_s} [g_{\rho,n}(\tilde{\mathbf{u}}^\tau, \boldsymbol{\delta}^\tau[s]) - V_{\max} + z_n^\tau]_+ \leq z_n^\tau \epsilon \tag{22b}$$

$$\frac{1}{N_s} \sum_{s=1}^{N_s} [V_{\min} - g_{\rho,n}(\tilde{\mathbf{u}}^\tau, \boldsymbol{\delta}^\tau[s]) + y_n^\tau]_+ \leq y_n^\tau \epsilon \tag{22c}$$

$$\frac{1}{N_s} \sum_{s=1}^{N_s} C_{c,n}^\tau(\mathbf{u}_n^\tau, \boldsymbol{\delta}^\tau[s]) \leq w_n^\tau \tag{22d}$$

$$\frac{1}{N_s} \sum_{s=1}^{N_s} \left[((1-\alpha_n^\tau) P_{\text{av},n}^\tau[s])^2 + (Q_n^\tau)^2 - S_n^2 + x_i^\tau\right]_+ \leq x_n^\tau \eta \tag{22e}$$

$$0 \leq \alpha_n^\tau \leq 1 \tag{22f}$$

$$B_n^{\tau+1} = B_n^\tau + \eta P_{B,n}^\tau \Delta^t \tag{22g}$$

$$P_{B,n}^{\min} \leq P_{B,n}^t \leq P_{B,n}^{\max} \tag{22h}$$

$$B_n^{\min} \leq B_n^t \leq B_n^{\max} \tag{22i}$$

$$\tilde{\mathbf{u}}_n^\tau = \mathbf{u}_n^\tau \quad \forall i \in \mathcal{N}_C, \tau \in \mathcal{T} \tag{22j}$$

where constraints (22d)–(22c) pertain to the utility, (22d)–(22i) are constraints for each customer i, and the consensus constraints (22j) ensure that utility and customer agree on the setpoints, while pursuing their own optimization objectives. Notice that variable $\tilde{\mathbf{u}}^\tau$ appears in the cost functions of the utility, as well as in the voltage regulation constraints. On the other hand, $\mathbf{u}_i^\tau$ is the argument of objective function and constraints for customer i. Following a procedure similar to e.g., [38], [39], the next step involves the introduction of auxiliary variables to facilitate the decomposability of the consensus constraints (22j) across utility and customers when an augmented Lagrangian function is considered. Then, by leveraging ADMM, it can be shown that the distributed algorithm boils down to the steps [S1]-[S2] performed iteratively as described below (i represent the iteration index).

[S1a] Variables $\{\tilde{\mathbf{u}}^\tau[i+1]\}_{\tau \in \mathcal{T}}$ are updated at the utility by solving the following problem:

$$\min_{\substack{\{\tilde{\mathbf{u}}^\tau\} \\ \{\tilde{w}^\tau\}, \{z_n^\tau, y_n^\tau\}}} \sum_{\tau=1}^{t+T} (\tilde{w}^\tau + R_u^\tau(\tilde{\mathbf{u}}^\tau, i))$$

$$\text{subject to}$$

$$\frac{1}{N_s} \sum_{s=1}^{N_s} C_u^\tau(\tilde{\mathbf{u}}^\tau, \boldsymbol{\delta}^\tau[s]) \leq \tilde{w}^\tau, \quad \forall \tau \in \mathcal{T}_t \tag{23a}$$

$$\frac{1}{N_s} \sum_{s=1}^{N_s} [g_{\rho,n}(\tilde{\mathbf{u}}^\tau, \boldsymbol{\delta}^\tau[s]) - V_{\max} + z_n^\tau]_+ \leq z_n^\tau \epsilon \tag{23b}$$

$$\frac{1}{N_s} \sum_{s=1}^{N_s} [V_{\min} - g_{\rho,n}(\tilde{\mathbf{u}}^\tau, \boldsymbol{\delta}^\tau[s]) + y_n^\tau]_+ \leq y_n^\tau \epsilon \tag{23c}$$

where constraints (23b)–(23c) are enforced for all $n \in \mathcal{N}, \tau \in \mathcal{T}_t$, and the iteration-dependent function $R_u(\tilde{\mathbf{u}}^\tau, i)$ is given by

$$R_u^\tau := \sum_{\tau \in \mathcal{T}} \sum_{n \in \mathcal{N}_C} \frac{\kappa}{2} \|\tilde{\mathbf{u}}_n^\tau\|_2^2 + (\tilde{\mathbf{u}}_n^\tau)^\mathsf{T} \left(\boldsymbol{\gamma}_n^\tau[i] - \frac{\kappa}{2} \tilde{\mathbf{u}}_n^\tau[i] - \frac{\kappa}{2} \mathbf{u}_n^\tau[i] \right). \tag{24}$$

[S1b] Setpoints $\mathbf{u}_n^\tau[i+1]$ for RES and battery located at customer $n \in \mathcal{N}_C$ are updated as:

$$\min_{\{\mathbf{u}_n^\tau, \mathbf{b}_n^\tau\} \{w_n^\tau\}, \{x_n^\tau\}} \sum_{\tau=t}^{t+T} \left(w_n^\tau + R_{c,n}^\tau(\mathbf{u}_n^\tau, i) \right)$$

$$\text{subject to}$$

$$\frac{1}{N_s} \sum_{s=1}^{N_s} C_{c,n}^\tau(\mathbf{u}_n^\tau, \boldsymbol{\delta}^\tau[s]) \leq w_n^\tau \quad \forall \tau \in \mathcal{T}_t \tag{25a}$$

$$\frac{1}{N_s} \sum_{s=1}^{N_s} \left[((1-\alpha_n^\tau) P_{\text{av},n}^\tau[s])^2 + (Q_n^\tau)^2 - S_n^2 + x_n^\tau\right]_+ \leq x_n^\tau \eta \quad \forall \tau \in \mathcal{T}_t \tag{25b}$$

$$0 \leq \alpha_n^\tau \leq 1 \quad \forall \tau \in \mathcal{T}_t \tag{25c}$$

$$B_n^{\tau+1} = B_n^\tau + \eta P_{B,n}^\tau \Delta^t \quad \forall \tau \in \mathcal{T}_t' \tag{25d}$$

$$P_{B,n}^{\min} \leq P_{B,n}^t \leq P_{B,n}^{\max} \quad \forall \tau \in \mathcal{T}_t' \tag{25e}$$

$$B_n^{\min} \leq B_n^t \leq B_n^{\max} \quad \forall \tau \in \mathcal{T}_t' \tag{25f}$$

where the iteration-dependent scalar function $R_{c,n}(\mathbf{u}_n^\tau, i)$ is given by:

$$R_{c,n}^\tau := \sum_{\tau \in \mathcal{T}} \frac{\kappa}{2} \|\mathbf{u}_n^\tau\|_2^2 - (\mathbf{u}_n^\tau)^\mathsf{T} \left(\boldsymbol{\gamma}_n^\tau[i] - \frac{\kappa}{2} \tilde{\mathbf{u}}_n^\tau[i] - \frac{\kappa}{2} \mathbf{u}_n^\tau[i] \right). \tag{26}$$

[S2] Dual variables $\{\boldsymbol{\gamma}_n^\tau[i+1]\}$ are updated as:

$$\boldsymbol{\gamma}_n^\tau[i+1] = \boldsymbol{\gamma}_n^\tau[i] + \frac{\kappa}{2} \left(\tilde{\mathbf{u}}_n^\tau[i+1] - \mathbf{u}_n^\tau[i+1] \right) \tag{27}$$

for all $n \in \mathcal{N}_C$ and $\tau \in \mathcal{T}$.

Algorithm 1 **Distributed architecture: DSO operation**

Generate $\{\boldsymbol{\delta}^\tau[s]\}$ and transmit $\{P^\tau_{\text{av},n}[s]\}$ to each customer n.
for $i = 1, 2, 3, \ldots$ until convergence **do**
  [s1] Transmit $\{\tilde{\mathbf{u}}^\tau[i]\}_{\tau\in\mathcal{T}}$ to customer n. Repeat $\forall n \in \mathcal{N}_C$.
  [s2] Receive $\{\mathbf{u}^\tau_n[i]\}_{\tau\in\mathcal{T}}$ from customer n. Repeat $\forall n \in \mathcal{N}_C$.
  [s3] Update $\{\tilde{\mathbf{u}}^\tau[i+1]\}_{\tau\in\mathcal{T},n\in\mathcal{N}_C}$ by solving (23).
  [s4] Update dual variables via (27).
  Go to [S1]
end for

Algorithm 2 **Distributed architecture: customer operation**

Receive $\{\boldsymbol{\delta}^\tau[s]\}$ from DSO.
for $i = 1, 2, 3, \ldots$ until convergence **do**
  [s1] Receive $\{\tilde{\mathbf{u}}^\tau[i]\}_{\tau\in\mathcal{T}}$ from DSO.
  [s2] Transmit $\{\mathbf{u}^\tau_n[i]\}_{\tau\in\mathcal{T}}$ to DSO.
  [s3] Update $\{\mathbf{u}^\tau[i+1]\}_{\tau\in\mathcal{T}}$ by solving (25).
  [s4] Update dual variables via (27).
  Go to [S1]
end for

Notice that problem (25) decouples into two subproblems, one in the variables $\{\alpha^\tau_n, Q^\tau_n\}_{\tau\in\mathcal{T}}$ and one in $\{P^\tau_{B,n}, b^\tau_n\}_{\tau\in\mathcal{T}}$ whenever functions $\{C^\tau_{c,n}(\cdot)\}$ decouple across variables.

Steps [S1]–[S2] above are repeated until convergence. A possible way to terminate the algorithm is to check the residuals $\|\tilde{\mathbf{u}}^\tau_n[i] - \mathbf{u}^\tau_n[i]\|_2$. At each iteration i, step [S1a] is performed at the distribution system operator (DSO), whereas step [S1b] is simultaneously computed at each customer n. Once [S1a] and [S1b] are performed, customers and DSO exchange the intermediate iterates $\mathbf{u}_n[i]$ and $\tilde{\mathbf{u}}_n[i]$ and carry out the update of the dual variables $\gamma_n[i]$. The complete list of steps performed at the DSO and at the customers at each iteration i is tabulated as Algorithm 1 and Algorithm 2.

Since (P2) is convex and constraints (22j) satisfy the conditions of [15, Prop. 4.2], convergence of the algorithm to the solution of (P2) is guaranteed; since (P2) is equivalent to (P1), the algorithm returns a solution of (P1) too. In the MPC strategy outlined in Section III-B, the distributed algorithm is utilized to solve (P1) over the horizon $\mathcal{T}$ in [A3]. Steps [S1]–[S2] are performed until convergence and, setpoints $\mathbf{u}^t_n$ are commanded to each RES and battery units.

V. Numerical tests

A. System setup

A modified version of the IEEE-37 node test feeder is utilized to test the proposed adaptive OPF method. As shown in Fig. 1, the modified network is obtained by considering the phase "c" and by replacing the loads specified in the original dataset with real load data measured from feeders near Sacramento, CA during the month of August 2012 [40]. The total loading of the feeder can be seen in Fig. 2, with a five-minute granularity. Other network data, such as line impedances, shunt admittances, and active and reactive loads are adopted from the respective dataset. It is assumed that twenty-one photovoltaic (PV) systems are placed at nodes 4, 7, 9, 10, 11, 13, 16, 17, 20, 22, 23, 26, 28, 29, 30, 31, 32, 33, 34, 35, and 36, and their generation profile is simulated based on the solar irradiance data available in [40]. The capacities are selected in a way to represent utility-scale PV systems,

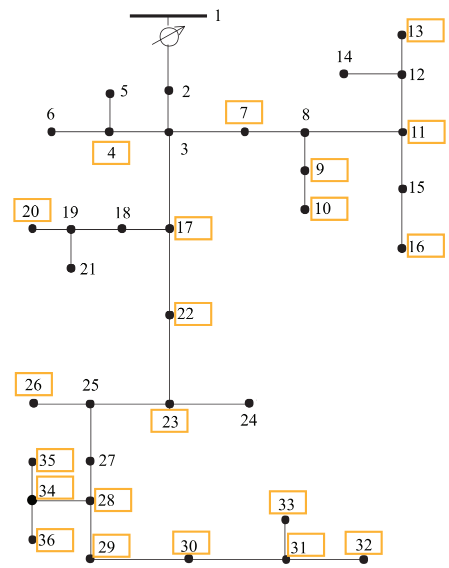

Fig. 1. IEEE 37-node test feeder considered in the test cases. Squares indicate nodes where PV systems are located.

TABLE III
Capacities of PV and storage systems in the considered simulation setup.

PV system		Battery	
Node	S_i [kVA]	Node	$B_i^{\max}$ [kWh]
4	100	9	100
7	200	10	100
9	200	28	50
10	400	29	250
11	440	32	250
13	240	35	120
16	400	36	200
17	240		
20	300		
22	100		
23	500		
26	200		
28	500		
29	200		
30	240		
31	400		
32	220		
33	500		
34	300		
35	300		
36	300		

roof-top PV systems for commercial facilities, or lump the capacities of PV systems on 10-15 houses connected to the same step-down transformer. The PV locations and capacities are summarized in Table III. For each receding horizon optimization, 130 samples were used from each random quantity in the calculation of the chance constraints. The aggregate available power $\sum_n P^\tau_{\text{av},n}$ during the course of the day is shown in Fig. 2. In these simulations, the voltage limits $V_{\max}$ and $V_{\min}$ are set to 1.05 pu and 0.95 pu, respectively.

When considering this level of PV penetration, overvoltage conditions can be observed during the hours of solar peak irradiation. By utilizing energy storage systems, model predictive control, and advanced inverter functionality, the overvoltages are mitigated. Similar to e.g., [1] energy storage units are co-located with the PV systems at nodes 9, 10, 28, 29, 32, 35, and 36, and their energy capacities $B_n^{\max}$ are assumed to be 100, 100, 50, 250, 250, 120, and 200 kWh, respectively. They represent community-scale energy storage systems, commercial-scale storage systems, or the capacity of 10-12 residential-scale batteries lumped into a single node. The minimum state of charge, $B_n^{\min}$ is set to zero for all batteries. The cost function is set to

$$\begin{aligned} C^\tau(\boldsymbol{\alpha}^\tau, \mathbf{q}_c^\tau, \mathbf{p}_B^\tau, \boldsymbol{\delta}^\tau) = \sum_{i \in \mathcal{N}} c_i^\tau [P_{\ell,n}^\tau + P_{B,n}^\tau - (1-\alpha_n^\tau) P_{\text{av},n}^\tau]_+ \\ + \sum_{i \in \mathcal{N}} d_i^\tau [(1-\alpha_n^\tau) P_{\text{av},n}^\tau - P_{\ell,n}^\tau - P_{B,n}^\tau]_+ \\ + \sum_{i \in \mathcal{N}} e_i^\tau |Q_n^\tau| + \sum_{i \in \mathcal{N}} f_i^\tau \alpha_i^\tau P_{\text{av},n}^\tau \end{aligned} \tag{28}$$

for all $\tau = t, \ldots, t+T$, where $c_i^\tau = 10$, $d_i^\tau = 3$, $e_i^\tau = 3$, and $f_i^t = 6$. Cost $C^t(\boldsymbol{\alpha}^t, \mathbf{q}_c^t, \mathbf{p}_B^t, \boldsymbol{\delta}^t)$ captures the price associated with the power consumed by the customers, as well as the feed-in tariff cost to the utility [1], the cost of reactive power injection/absorption from the inverters, and the cost of active power curtailment. The parameter ϵ is fixed to 0.01 in the probabilistic constraints; i.e., a 1% violation of probabilistic constraints is allowed in the optimization.

Each energy storage device is set to have a maximum five-minute charge rate of 10% of their respective energy capacities, $B_n^{\max}$. Forecasting errors for load and available active power are assumed to follow a truncated Gaussian distribution, with the distribution truncated at $\pm 3\sigma$, with σ denoting the standard deviation. The standard deviation of the forecasting errors is assumed to be 3% of the actual value for the first hour in the prediction and 7% for future timesteps. Two test cases are considered here: (C1) 2 hours, with a granularity of 5 minutes during the first hour and 15 minutes during the second hour; and, (C2) 2 hours with the same granularity as before, but using a (deterministic) certainty equivalent formulation where the forecasted available powers and loads are utilized in the MPC strategy. Particularly, for (C2) the voltage constraints in (P1) are reformulated into simpler deterministic constraints where the forecasted values of loads and available power from PV systems are utilized. The solver SDPT3 is utilized to solve the optimization problems in MATLAB. The solver took 1.7 seconds to solve the centralized multi-period OPF over 12 time instants on a Macbook Pro laptop with 16 GB of memory and 2.8 Ghz Intel Core i7. An implementation of the distributed ADMM algorithm described in Section IV will require longer computation times from multiple iterations and communication delays but allows decomposition of the computations across customers and the utility.

B. Approximation accuracy

First, the accuracy of the voltage approximation is tested in two cases: i) no RES generation (Case I) and ii) in the presence of reverse power flow (Case II). Fig. 3 shows the actual voltage profile as well as the voltage magnitudes across

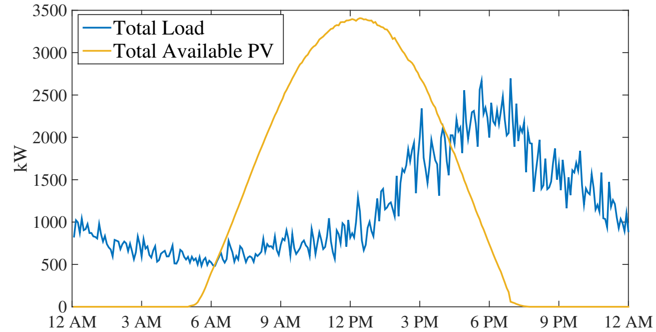

Fig. 2. Total feeder loading and available PV generation.

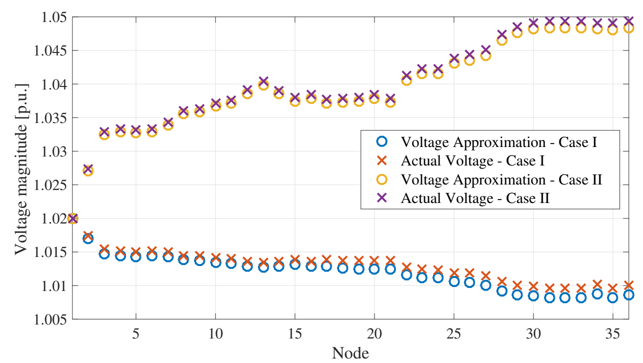

Fig. 3. Actual and approximated values of the voltage magnitude. The linearized model closely approximates the actual nonlinear powerflow.

the nodes obtained by using the linearized model explained in Section II-B. It can be seen that the approximation is accurate in both cases. See e.g., [10], [12] for additional numerical results as well as analytical bounds for the approximation errors.

C. Example of performance of the proposed method

A sample of the voltage profiles achieved with (C1) is provided in Fig. 4. It can be seen that the voltages are confined within the desired limits. This will be further confirmed shortly when describing the results provided by Fig. 7. The state of charge of the batteries are shown in Fig. 5, and the corresponding charging/discharging pattern for each battery is shown in Fig. 6, demonstrating the charging of the batteries during peak solar irradiance times and discharging as the available solar energy decreases. When avoiding curtailment, the batteries charge at their maximum charge rate and the batteries become fully charged for a small amount of time.

Fig. 7 compares snapshots of the voltage profiles obtained with strategies (C1), (C2), and in the vase where no active power curtailment or reactive power strategies are implemented. Voltage profiles correspond to 12PM. The strategy (C2) is tested for three different realizations of the forecasting errors: i) in case of perfect forecast, which serves as a benchmark; ii) when the available active power from the PV system is underestimated by 10%; and, iii) when the available active power from the PV system is overestimated by 10%. It is

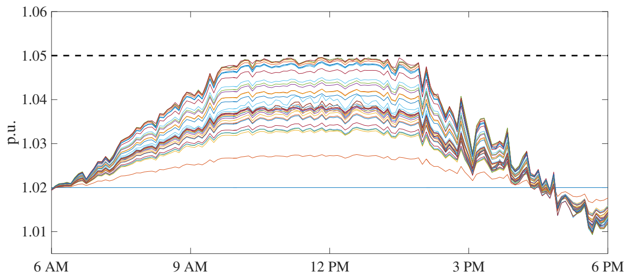

Fig. 4. Voltage profile achieved with the chance-constrained OPF method in the considered test case.

clearly seen that when no active power curtailment or reactive power strategies are implemented the voltages exceed the limit of 1.05 pu at a number of nodes. The strategy (C2) based on the certainty equivalent formulation works well when the forecast is perfect, and the only factor affecting the voltage profile is the error in the linear approximation of the AC power-flow equations. However, (C2) leads to overvoltage conditions when the power available from the PV is underestimated, and to an over-conservative solution when $P^{\tau}_{\text{av},i}$ is overestimated. The proposed chance-constrained approach is more conservative, but drives the voltage magnitudes within the desired range in spite of forecasting errors.

Figure 8 illustrates the probability distribution of the voltage magnitudes for strategies (C1) and (C2). Recall that the forecasting errors for load and available active power from the PV systems are assumed to follow a truncated Gaussian distribution, with the distribution truncated at $\pm 3\sigma$, with σ denoting the standard deviation. For the test reported in Figure 8, the truncated Gaussian distribution is centered around the true values of loads and available active powers. The standard deviation of the forecasting errors is assumed to be 3% of the actual value for the first hour in the prediction and 7% for future timesteps. As expected, it can be seen that the proposed strategy (C1) leads to a less frequent violation of the voltage magnitudes. Particularly, the upper limit on the voltage magnitudes is violated 0.74% of the time, which satisfies the maximum violation probability of 1% specified in the chance-constraints. On the other hand, strategy (C2) leads to a violation probability larger than 2% even if the truncated Gaussian distribution is centered around the true values of loads and available active powers.

VI. Concluding Remarks

The paper developed an adaptive AC OPF approach to optimize the operation of distribution systems featuring RESs and energy storage devices under forecasting errors. Controllability of output active and reactive power is presumed for RESs. The proposed method utilizes a chance-constrained multi-period AC OPF formulation, where probabilistic constraints are utilized to enforce voltage regulation with a prescribed probability. To enable a computationally affordable convex reformulation, a linear approximation of the AC power-flow equations was utilized, along with conservative approximations for the chance constraints. An adaptive optimization

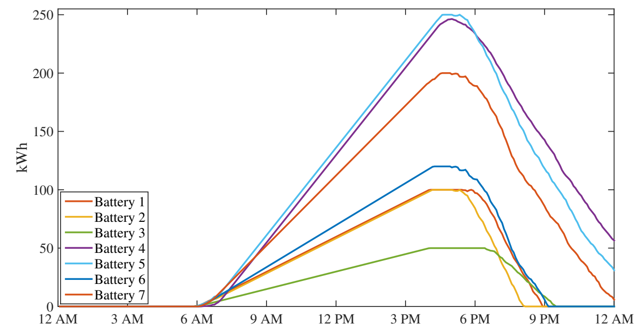

Fig. 5. State of charge of the batteries over time.

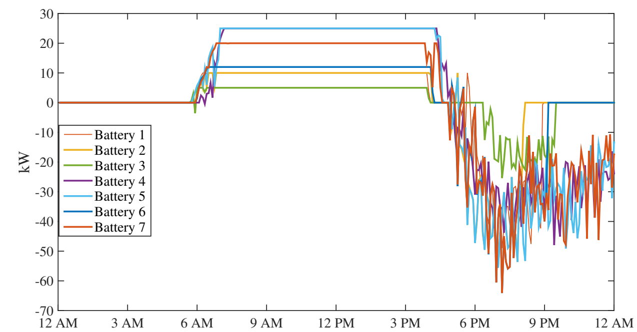

Fig. 6. Power dis/charged from each battery.

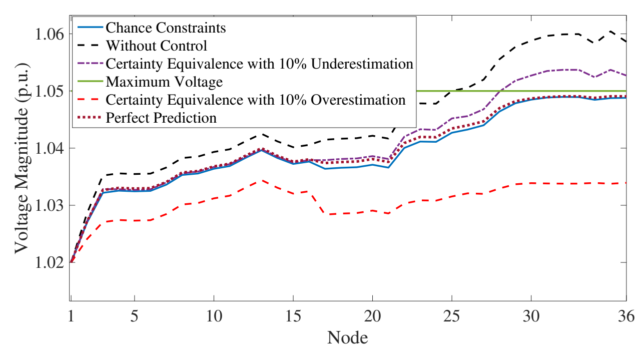

Fig. 7. Comparison of voltage profiles achieved at 12PM using the proposed method, MPC with forecasted irradiance and loads, and no controls.

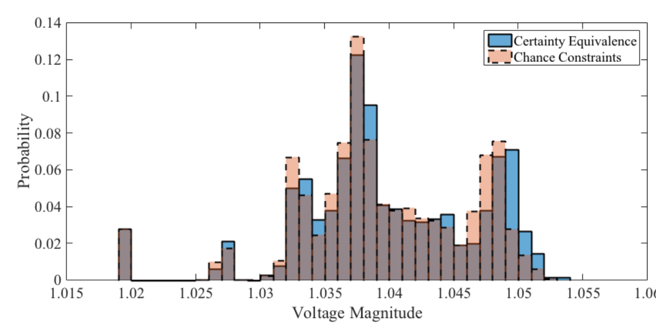

Fig. 8. Probability distribution of voltage magnitudes for strategies (C1) and (C2).

strategy was then obtained via receding horizon control. A distributed solution strategy was developed to enable utility and customers to pursue their own optimization objectives, while ensuring that voltage constraints are satisfied. Future efforts will explore alternative linearization techniques for the AC power-flow equations, convex approximation techniques for chance constraints that are robust to inaccuracies in the forecasting error distribution, strategies for learning and improving forecast error distribution models from empirical operational data, and translating probabilistic constraint satisfaction guarantees from the linearized to the full nonlinear model.

REFERENCES

[1] J. von Appen, T. Stetz, M. Braun, and A. Schmiegel, "Local voltage control strategies for PV storage systems in distribution grids," *IEEE Trans. on Smart Grid*, vol. 5, no. 2, pp. 1002–1009, March 2014.

[2] P. Jahangiri and D. C. Aliprantis, "Distributed Volt/VAr control by PV inverters," *IEEE Trans. Power Syst.*, vol. 28, no. 3, pp. 3429–3439, Aug. 2013.

[3] E. Dall'Anese, S. V. Dhople, and G. B. Giannakis, "Optimal dispatch of photovoltaic inverters in residential distribution systems," *IEEE Trans. Sust. Energy*, vol. 5, no. 2, pp. 487–497, Apr. 2014.

[4] A. Samadi, R. Eriksson, L. Soder, B. G. Rawn, and J. C. Boemer, "Coordinated active power-dependent voltage regulation in distribution grids with PV systems," *IEEE Trans. on Power Del.*, vol. 29, no. 3, pp. 1454–1464, June 2014.

[5] Y. Liu, J. Bebic, B. Kroposki, J. de Bedout, and W. Ren, "Distribution system voltage performance analysis for high-penetration PV," in *IEEE Energy 2030 Conf.*, Nov. 2008.

[6] P. Malysz, S. Sirouspour, and A. Emadi, "An optimal energy storage control strategy for grid-connected microgrids," *IEEE Trans. on Smart Grid*, vol. 5, no. 4, pp. 1785–1796, July 2014.

[7] S. Paudyaly, C. A. Canizares, and K. Bhattacharya, "Three-phase distribution OPF in smart grids: Optimality versus computational burden," in *2nd IEEE PES Intl. Conf. and Exhibition on Innovative Smart Grid Technologies*, Manchester, UK, Dec. 2011.

[8] A. Nemirovski and A. Shapiro, "Convex approximations of chance constrained programs," *SIAM J. on Optimization*, vol. 17, no. 4, pp. 969–996, 2007.

[9] M. E. Baran and F. F. Wu, "Network reconfiguration in distribution systems for loss reduction and load balancing," *IEEE Trans. on Power Delivery*, vol. 4, no. 2, pp. 1401–1407, Apr. 1989.

[10] S. Dhople, S. Guggilam, and Y. Chen, "Linear approximations to ac power flow in rectangular coordinates," *Allerton Conference on Communication, Control, and Computing , in Press*, 2015.

[11] S. Bolognani and F. Dörfler, "Fast power system analysis via implicit linearization of the power flow manifold," in *2015 53rd Annual Allerton Conf. on Communication, Control, and Computing*, 2015, pp. 402–409.

[12] S. Guggilam, E. Dall'Anese, Y. Chen, S. Dhople, and G. B. Giannakis, "Scalable optimization methods for distribution networks with high pv integration," *IEEE Transactions on Smart Grid*, 2016.

[13] S. Bolognani and S. Zampieri, "On the existence and linear approximation of the power flow solution in power distribution networks," *IEEE Transactions on Power Systems*, vol. 31, no. 1, pp. 163–172, Jan. 2016.

[14] G. Calafiore and L. El Ghaoui, "On distributionally robust chance constrained linear programs," *Journal of Optimization Theory and Applications,*, vol. 130, no. 1, pp. 1–22, 2006.

[15] D. P. Bertsekas and J. N. Tsitsiklis, *Parallel and Distributed Computation: Numerical Methods*. Englewood Cliffs, NJ: Prentice Hall, 1989.

[16] A. Parisio and L. Glielmo, "Stochastic model predictive control for economic/environmental operation management of microgrids," in *IEEE European Control Conference*, Zürich, Switzerland, 2013.

[17] P. Fortenbacher, A. Ulbig, S. Koch, and G. Andersson, "Grid-constrained optimal predictive power dispatch in large multi-level power systems with renewable energy sources, and storage devices," in *IEEE PES Innovative Smart Grid Technologies Conference Europe*, Istanbul, Turkey, Oct. 2014.

[18] F. Adamek, M. Arnold, and G. Andersson, "On decisive storage parameters for minimizing energy supply costs in multicarrier energy systems," *IEEE Trans. on Sustainable Energy*, vol. 5, no. 1, pp. 102–109, Jan 2014.

[19] R. A. Jabr, S. Karaki, and J. A. Korbane, "Robust multi-period OPF with storage and renewables," *IEEE Trans. Power Syst.*, vol. 30, no. 5, pp. 2790–2799, Sept 2015.

[20] J. Warrington, P. Goulart, S. Mariethoz, and M. Morari, "Policy-based reserves for power systems," *IEEE Trans. on Power Systems*, vol. 28, no. 4, pp. 4427–4437, Nov 2013.

[21] D. Bienstock, M. Chertkov, and S. Harnett, "Chance-constrained optimal power flow: Risk-aware network control under uncertainty," *SIAM Review*, vol. 56, no. 3, pp. 461–495, 2014.

[22] T. Summers, J. Warrington, M. Morari, and J. Lygeros, "Stochastic optimal power flow based on conditional value at risk and distributional robustness," *International Journal of Electrical Power & Energy Systems*, vol. 72, pp. 116–125, Nov. 2015.

[23] M. Lubin, Y. Dvorkin, and S. Backhaus, "A robust approach to chance constrained optimal power flow with renewable generation," *IEEE Transactions on Power Systems (in press)*, 2015.

[24] L. Roald, S. Misra, M. Chertkov, and G. Andersson, "Optimal power flow with weighted chance constraints and general policies for generation control," 2015, [Online] Available at: http://arxiv.org/pdf/1504.00057.

[25] D. Gayme and U. Topcu, "Optimal power flow with large-scale storage integration," *IEEE Trans. Power Syst.*, vol. 28, pp. 709–717, 2012.

[26] E. Dall'Anese, S. V. Dhople, B. B. Johnson, and G. B. Giannakis, "Optimal dispatch of residential photovoltaic inverters under forecasting uncertainties," *IEEE J. of Photovoltaics*, vol. 5, no. 1, pp. 350–359, Jan 2015.

[27] W. H. Kersting, *Distribution System Modeling and Analysis*. 2nd ed., Boca Raton, FL: CRC Press, 2007.

[28] J. Lavaei and S. H. Low, "Zero duality gap in optimal power flow problem," *IEEE Trans. Power Syst.*, vol. 27, no. 1, pp. 92–107, Feb. 2012.

[29] H. Zhang, V. Vittal, G. Heydt, and J. Quintero, "A relaxed ac optimal power flow model based on a taylor series," in *IEEE Innovative Smart Grid Technologies-Asia*, 2013.

[30] R. Madani, M. Ashraphijuo, and J. Lavaei, "Promises of conic relaxation for contingency-constrained optimal power flow problem," in *52nd Annual Allerton Conference on Communication, Control, and Computing*, 2014, pp. 1064–1071.

[31] C. Coffrin, H. Hijazi, and y. P. Van Hentenryck, "The qc relaxation: Theoretical and computational results on optimal power flow."

[32] W. Wang and S. Ahmed, "Sample average approximation of expected value constrained stochastic programs," *Operations Research Letters*, vol. 36, no. 5, pp. 515–519, 2008.

[33] W.-K. Mak, D. Morton, and R. Wood, "Monte carlo bounding techniques for determining solution quality in stochastic programs," *Operations Research Letters*, vol. 24, no. 1, pp. 47–56, 1999.

[34] A. Shapiro, "Monte carlo sampling methods," *Handbooks in operations research and management science*, vol. 10, pp. 353–425, 2003.

[35] J. Linderoth, A. Shapiro, and S. Wright, "The empirical behavior of sampling methods for stochastic programming," *Annals of Operations Research*, vol. 142, no. 1, pp. 215–241, 2006.

[36] K. Rahbar, J. Xu, and R. Zhang, "Real-time energy storage management for renewable integration in microgrid: An off-line optimization approach," *IEEE Trans. Smart Grid*, vol. 6, no. 1, pp. 124–134, Jan. 2015.

[37] M. Cannon, B. Kouvaritakis, S. V. Raković, and Q. Cheng, "Stochastic tubes in model predictive control with probabilistic constraints," *IEEE Transactions on Automatic Control*, vol. 56, no. 1, pp. 194–200, 2011.

[38] E. Dall'Anese, H. Zhu, and G. B. Giannakis, "Distributed optimal power flow for smart microgrids," *IEEE Trans. Smart Grid*, vol. 4, no. 3, pp. 1464–1475, Sep. 2013.

[39] S. Boyd, N. Parikh, E. Chu, B. Peleato, and J. Eckstein, "Distributed optimization and statistical learning via the alternating direction method of multipliers," *Foundations and Trends in Machine Learning*, vol. 3, no. 1, pp. 1–122, 2011.

[40] J. Bank and J. Hambrick, "Development of a high resolution, real time, distribution-level metering system and associated visualization modeling, and data analysis functions," National Renewable Energy Laboratory, Tech. Rep. NREL/TP-5500-56610, May 2013.

Emiliano Dall'Anese (S'08-M'11) received the Laurea Triennale (B.Sc Degree) and the Laurea Specialistica (M.Sc Degree) in Telecommunications Engineering from the University of Padova, Italy, in 2005 and 2007, respectively, and the Ph.D. in Information Engineering from the Department of Information Engineering, University of Padova, Italy, in 2011. From January 2009 to September 2010, he was a visiting scholar at the Department of Electrical and Computer Engineering, University of Minnesota, USA. From January 2011 to November 2014 he was a Postdoctoral Associate at the Department of Electrical and Computer Engineering and Digital Technology Center of the University of Minnesota, USA. Since December 2014 he has been a Senior Engineer at the National Renewable Energy Laboratory, Golden, CO, USA.

His research interests lie in the areas of optimization, signal processing, and control. Application domains include power systems and communications. Current efforts focus on distributed optimization and control of power distribution systems with distributed (renewable) energy resources and statistical inference for grid data analytics.

Kyri Baker (S'08-M'15) received the B.S., M.S., and Ph.D. degrees in electrical and computer engineering from Carnegie Mellon University, in 2009, 2010, and 2014, respectively. She spent a year as a postdoctoral researcher at the National Renewable Energy Laboratory (NREL) in Golden, CO in the Residential Buildings group, and presently she is a Research Engineer in the Power Systems Engineering Center at NREL. Her research interests include power systems optimization, smart buildings, and renewable energy integration.

Tyler Summers is an Assistant Professor of Mechanical Engineering with an affiliate appointment in Electrical Engineering at the University of Texas at Dallas. Prior to joining UT Dallas, he was an ETH Postdoctoral Fellow at the Automatic Control Laboratory at ETH Zurich from 2011 to 2015. He received a B.S. degree in Mechanical Engineering from Texas Christian University in 2004 and an M.S. and PhD degree in Aerospace Engineering with emphasis on feedback control theory at the University of Texas at Austin in 2007 and 2010, respectively. He was a Fulbright Postgraduate Scholar at the Australian National University in Canberra, Australia in 2007-2008. His research interests are in feedback control and optimization in complex dynamical networks, with applications to electric power networks and distributed robotics.